DFT Vibrational Calculations of Rhodamine 6G Adsorbed on Silver: Analysis of Tip-Enhanced Raman Spectroscopy

Hiroyuki Watanabe,[†,‡] Norihiko Hayazawa,[∥] Yasushi Inouye,*[,§,∥] and Satoshi Kawata[†,∥]

Department of Applied Physics, Osaka University, Suita, Osaka 565-0871, Japan, Analysis Technology Center, Advanced Core Technology Laboratories, Fuji Photo Film Co., Ltd, Minami-Ashigara, Kanagawa 250-0193, Japan, Graduate School of Frontier Biosciences, Osaka University, Suita, Osaka 565-0871, Japan, and RIKEN, Wako, Saitama 351-0198, Japan

Received: September 17, 2004; In Final Form: January 10, 2005

The tip-enhanced near-field Raman (TERS) bands of Rhodamine 6G (R6G), that we reported earlier [*Chem. Phys. Lett.* **2001**, *335*, 369.], are assigned on the basis of density-functional theory (DFT) calculations at the 6-311++G(*d,p*) level. The Raman and infrared intensities as well as frequencies of the vibrational modes are used for band assignments. These vibrational modes, in combination with characterization of resonant electronic transitions using time-dependent DFT calculations, predict spectral changes in resonant Raman and surface-enhanced resonant Raman scatterings of R6G. Moreover, the TERS spectra of R6G are analyzed in detail, where interactions between the tip and R6G molecules and their enhancement mechanisms are discussed. Finally, we propose a novel Raman spectroscopy technique capable of detecting molecular vibrations at sub-nanometer scale.

1. Introduction

Near-field Raman spectroscopy[1−7] facilitates detection of molecular vibrations in nanometric scale, smaller than the diffraction limit of the light.[8−12] We have obtained near-field Raman spectra of several nano materials,[4,5,13−16] using a metallic probe tip that generates local plasmon polariton excitation[17−21] at the vicinity of the tip apex. These tip-enhanced near-field Raman scattering (TERS) spectra are often different from the conventional micro-Raman (far-field Raman) scattering spectra. For example, we obtained TERS spectra of single adenine nanocrystals, where, owing to the deformation of adenine molecule pressurized by the metallic probe tip,[16] frequency shifts of the TERS bands were observed. Furthermore, we demonstrated TERS spectra of polycrystalline Rhodamine 6G (R6G) molecules (Figure 1) dispersed on a silver island film by using the silver-coated probe tip.[13,14] These spectra involve anomalous enhancement in intensity of some specific Raman peaks against conventional surface enhancement resonance Raman scattering (SERRS) spectra obtained from the same sample. We concluded in the report that the metallic tip provides additional enhancement and insights into SERRS and that the evidence of tip−molecule chemical interaction is provided.[13]

The R6G has been utilized for a probe molecule in the field of extremely high sensitive detections, such as single molecule detection using SERRS effects,[22−28] nonlinear vibrational detection using hyper-Raman scattering[29] as well as IR−UV−vis sum frequency generation,[30] and nanometer scale detection using near-field Raman spectroscopy.[13,31,32] As for the assignment of the vibrational modes of the R6G molecule, to the best of our knowledge, only one report by Hildebrandt et al.[33] has been quoted. However, this assignment seems to be partial and has a few questionable modes. Hence, it would be considerably difficult to estimate the precise picture of chemical interactions between R6G and the surrounding areas.

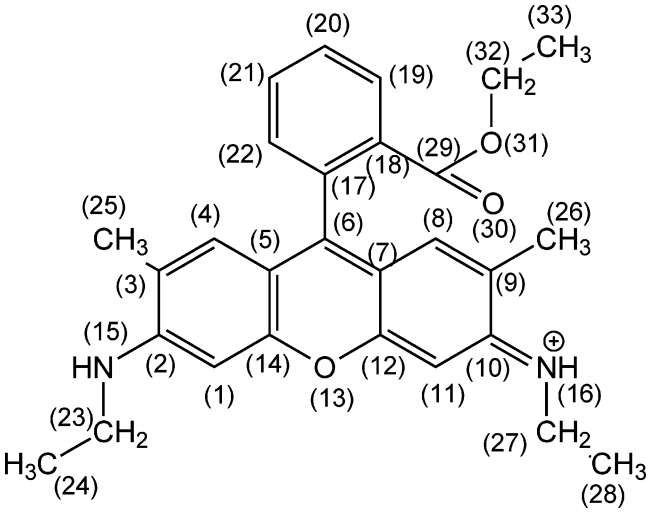

Figure 1. Molecular structure and atomic numbering of R6G.

In this paper, we report the full assignment on the vibrational modes of the R6G molecule by performing high-level density functional theory (DFT) vibrational calculations in the first part. We then analyze the TERS spectra of R6G in comparison with conventional resonant Raman scattering (RRS) and SERRS spectra that are recorded under the same conditions of excitation frequency and sample preparation. We also estimate the interactions between the probe tip and the molecules in the final part.

2. Experimental and Computational Procedures

The R6G {xanthylium, 9-[2-(ethoxycarbonyl)phenyl]-3,6-bis-(ethylamino)- 2,7-dimethyl-, chloride} was purchased from the

* Author to whom correspondence should be addressed. Phone: +81-6-6879-7847. Fax: +81-6-6879-7330. E-mail: ya-inoue@ap.eng.osaka-u.ac.jp.

† Department of Applied Physics, Osaka University.

‡ Analysis Technology Center, Advanced Core Technology Laboratories, Fuji Photo Film Co., Ltd.

§ Graduate School of Frontier Biosciences, Osaka University.

∥ RIKEN.

10.1021/jp045771u CCC: $30.25
Published on Web 02/26/2005

Wako Pure Chemical Industries, Ltd, and was not treated with any further purification.

In the present study, the infrared and Raman spectra of R6G were observed at the resolution of 1 cm^{-1}. Both in the SERRS and the TERS measurements, R6G molecules (2.6 mmol/L) dissolved in ethanol were cast and dried on a silver island film (thickness: 8 nm). In the measurement of the off-resonance Raman scattering as well as the RRS, R6G molecules (50 mmol/L and 50 μmol/L, respectively) dissolved in ethanol were used, with careful subtraction of solvent peaks. In the infrared measurement, R6G molecules in a KBr disk were employed.

Raman spectral measurements were performed with a Bruker RFS-100 Fourier transform Raman spectrometer by using 1064-nm wavelength of the Nd:YAG laser for Raman excitation (for the off-resonance Raman spectroscopy) in the region of 1800−200 cm^{-1}, and with a Jovin Yvon T-64000 conventional Raman spectrometer by using the 488-nm emission of an Ar-ion laser (both for the RRS and SERRS spectroscopy) in the region of 1800−200 cm^{-1}. The TERS spectra were recorded with our homemade near-field Raman scanning optical microscope (Raman NSOM) by using the 488-nm wavelength of an Ar-ion laser in the region of 1800−600 cm^{-1}. The Raman NSOM probe was an AFM cantilever tip coated with a 40-nm thick silver layer. The detailed optical setup of the Raman NSOM is described in our previous report.[13] Infrared spectra in the region of 1800−600 cm^{-1} were recorded on a BIO-RAD FTS-40 Fourier transform infrared spectrometer.

Quantum chemical calculations to analyze and identify the vibrational frequencies, normal modes, and Raman intensities for R6G molecule were carried out using the B3LYP functional[34,35] with the basis set of 6-311++G(*d,p*). The vibrational frequencies were uniformly scaled by a factor of 0.9982. This scale factor was obtained by taking the least-squares difference between theoretical and experimental frequencies in the region of 1800−600 cm^{-1}. The calculations for electronic excited states of the R6G molecule were performed by the time-dependent DFT (TD-DFT) method[36,37] using the B3LYP functional with the same basis set. These calculations were performed using the GAUSSIAN98 Revision A.9 program package.[38] The potential energy distributions (PED) for the vibrations were calculated using the existing program.[39] The optimized geometry and the calculated vibrational modes were visualized using the MOLDEN program (QCPE 619)[40] and the VLX program.[41,42]

Raman spectral searches against a reference database were performed within the KnowItAll Information System manufactured by Bio-Rad Laboratories. The database contains 4465 spectra of monomers, polymers, inorganic materials, and processing chemicals.

3. Results and Discussion

A. Molecular Structure of R6G. The molecular geometry of the cationic form of R6G was fully optimized in vacuo at the B3LYP/6-311++G(*d,p*) level from the crystal structure[43] as an initial geometry. The optimized geometry has no imaginary frequencies, thereby representing an energy minimum. These geometrical parameters are listed, together with the parameters of 4XD crystal structure,[43] in Table 1. Both the calculated and experimental geometries are also shown in Figure 2. The angle between the xanthene plane and its adjacent phenyl-ring plane is nearly perpendicular (87°) in the calculated geometry, whereas the angle in the crystal structure is distorted to 62°. The ethoxy carbonyl group adjacent to the phenyl ring also has a different orientation, with the dihedral angle of C29−O31−C32−C33 being parallel (0°) in the calculated geometry against being nearly perpendicular (94°) in the crystal structure. The conformational differences in the crystal and calculated structures are considered to be mainly due to the packing effect in the crystal because the crystalline rhodamine B,[43] which is less hindered in geometry than R6G, gives the same conformation as the calculated results of R6G. Therefore, the calculated geometry of R6G is employed for the further vibrational analysis.

TABLE 1: Optimized Bond Lengths (in Å), Bond Angles (in deg), and Dihedral Angles (in deg) of R6G at B3LYP/6-311++G(*d,p*) Level[a]

	4XD (Adhikesavalu et al.)[b]	calculated (B3LYP/6-311++G(*d,p*))
	Bond Lengths (Å)	
C1−C2	1.409	1.407
C1−C14	1.361	1.380
C2−C3	1.442	1.446
C2−N15	1.325	1.354
C3−C4	1.341	1.368
C3−C25	1.502	1.506
C4−C5	1.430	1.424
C5−C6	1.388	1.408
C5−C14	1.419	1.419
C6−C17	1.491	1.496
O13−C14	1.368	1.358
N15−C23	1.455	1.464
C17−C18	1.400	1.401
C17−C22	1.381	1.398
C18−C19	1.392	1.401
C18−C29	1.475	1.497
C19−C20	1.361	1.390
C20−C21	1.370	1.392
C21−C22	1.373	1.393
C23−C24	1.493	1.531
C29−O30	1.193	1.213
C29−O31	1.333	1.338
O31−C32	1.462	1.458
C32−C33	1.470	1.513
	Bond Angles (deg)	
C1−C2−C3	118.4	119.4
C1−C2−N15	122.1	121.7
C1−C14−C5	123.1	122.5
C1−C14−O13	116.6	116.7
C2−C3−C4	119.3	118.8
C2−C3−C25	119.8	120.0
C3−C4−C5	123.9	123.0
C4−C5−C6	125.3	124.4
C4−C5−C14	114.9	116.4
C5−C6−C7	119.3	119.1
C5−C6−C17	119.7	120.4
C12−O13−C14	120.2	121.0
N15−C23−C24	112.8	113.8
C17−C18−C19	119.3	119.4
C17−C18−C29	120.8	119.8
C17−C22−C21	121.8	120.9
C18−C19−C20	121.0	120.9
C18−C29−O30	125.2	123.7
C18−C29−O31	109.8	112.6
C19−C20−C21	120.2	119.7
C20−C21−C22	119.6	120.0
C29−O31−C32	117.5	116.9
O31−C32−C33	108.1	107.6
	Dihedral Angles (deg)	
C1−C2−N15−C23	−0.2	1.8
C2−N15−C23−C24	84.6	82.1
C5−C6−C17−C18	−118.3	−92.7
C11−C10−N16−C27	−2.9	−1.8
C17−C18−C29−O30	35.3	0.0
C29−O31−C32−C33	−93.6	−180.0

[a] Atom numbering as in Figure 1. [b] Ref 43.

B. Vibrational Analysis of R6G. The calculated frequencies of R6G were uniformly scaled by a factor of 0.9982. The corrected vibrational frequencies vs the off-resonant Raman frequencies of R6G in ethanol solution (Ex: 1064 nm) are listed

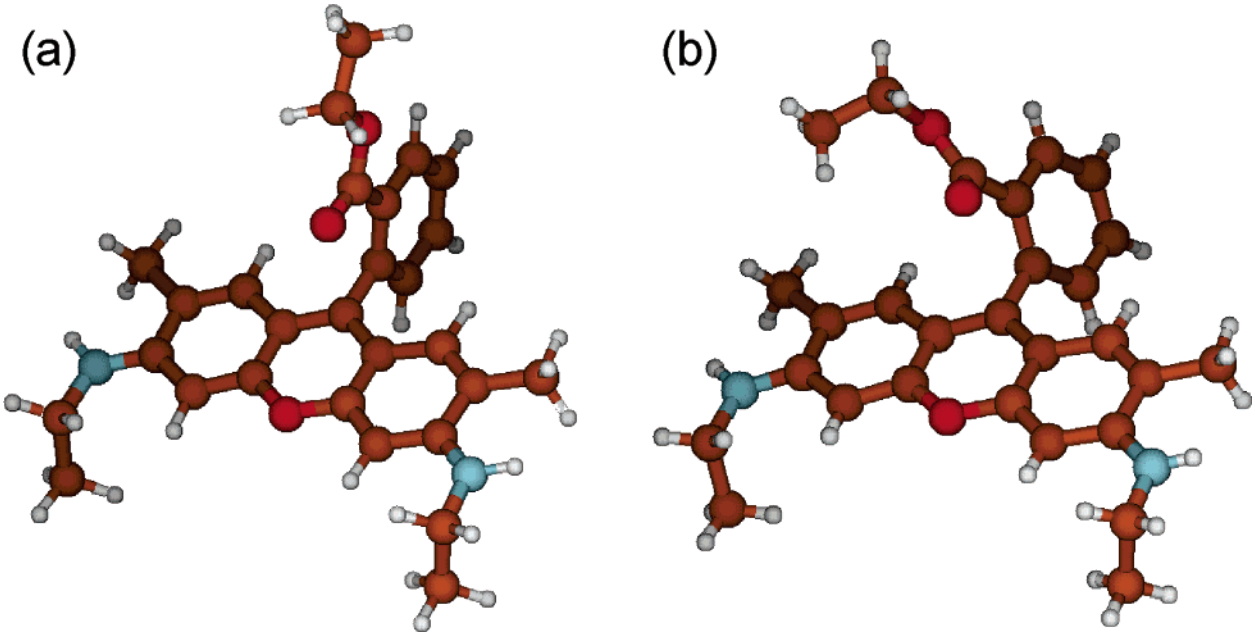

Figure 2. (a) Optimized geometry using B3LYP/6-311++G(*d*,*p*) level and (b) crystal structure of R6G.

in Table 2, together with the infrared absorption frequencies. This does not include the results relating to the CH stretching and the NH stretching modes having frequencies higher than 2800 cm^{-1}. The calculated frequencies uniformly scaled by a constant factor have a surprisingly good agreement with the experimental frequencies in the region of 1800−600 cm^{-1}; the differences between the calculated and experimental frequencies are smaller than 15 cm^{-1}. Judging from a general reliability[44−48] of the vibrational frequencies calculated with the high-level basis set as we employed, the accuracy would be high enough for the individual band assignments; however, still some bands are not uniquely assigned. A Raman band at 1389 cm^{-1} is assigned to degenerated vibrational modes of ν_{122}, ν_{123}, ν_{124}, and ν_{125}, which correspond to the symmetric bending motions of individual methyl groups. Three bands are assigned to alternative vibrational modes; that is, a band at 705 cm^{-1} is assigned to the calculated mode of either ν_{58} or ν_{59}, a band at 1061 cm^{-1} is due to the mode of either ν_{90} or ν_{91}, and 1490 cm^{-1} is either of ν_{140} or ν_{141}, respectively. In addition, extremely weak bands are left unassigned.

In a large molecule that contains several vibrational units such as R6G, vibrational modes are complicated as they contain motions of many atoms. We analyze the potential energy distribution (PED) for the vibrational modes, which are listed in Table 2. The percentage of the PED (PED%) are bounded into four regions of molecule: "X" represents the motion of the xanthene ring, "A" represents that of the two NHC_2H_5 groups, "M" represents that of the two methyl groups, and "P" represents that of the phenyl ring with the $COOC_2H_5$ group, respectively. Nine Raman bands with strong scattering intensities at 613, 775, 1130, 1278, 1364, 1389, 1512, 1577, and 1651 cm^{-1} are assigned to the corresponding vibrational modes ν_{53}, ν_{65}, ν_{96}, ν_{111}, ν_{117}, ν_{122}, ν_{146}, ν_{151}, and ν_{154}, respectively. These vibrational modes have some discrepancies to the former band assignments by Hildebrandt et al.,[33] as the vibrating regions of two vibrational modes (ν_{111} and ν_{122}) of our calculations do not agree with the former assignments.[33] The mode ν_{65} is an in-plane deformation of the xanthene ring in our calculations, while this mode was assigned to a C−H out-of-plane bend of the same xanthene ring in the former report. In addition, contribution of a symmetric in-plane C−H bend of the xanthene ring was not mentioned in the previous report of the vibrational mode ν_{154}. Consequently, the present calculation corrects the previous assignments of several important bands.

C. RRS and SERRS Spectra of R6G. Figure 3 shows RRS and SERRS spectra together with the off-resonance Raman spectrum of R6G. The RRS spectrum of R6G in ethanol solution (excitation wavelength = 488 nm) and the SERRS of R6G adsorbed on a silver island film (excitation wavelength = 488 nm) as well as the off-resonance Raman spectrum of R6G in ethanol solution (excitation wavelength = 1064 nm) are plotted versus corresponding frequencies in the region of 1800−200 cm^{-1}. These Raman frequencies and relative Raman intensities are summarized in Table 3, and their vibrational patterns are also shown in Figure 4. The RRS spectral pattern (Figure 3b) differs from the off-resonance Raman spectrum (Figure 3a). In particular, RRS bands at 657 cm^{-1} (ν_{55}), at 1577 cm^{-1} (ν_{151}), and at 1649 cm^{-1} (ν_{154}) exhibit specific intensity enhancement against the corresponding off-resonance Raman bands. Among these specific RRS bands, the band ν_{154} is mainly due to a C═C totally symmetric stretch of the xanthene ring. The vibrational modes of both bands ν_{55} and ν_{151} are localized in the phenyl ring, whereas the band ν_{55} is due to a symmetric deformation and the band ν_{151} is due to a C═C symmetric stretching motion, respectively. In principle, the intensities of the RRS bands depend on the nature of the resonant excited state; that is, only a vibrational mode which is active to vibrational transitions with electronic excitations between the ground and resonant excited states demonstrates RRS intensity enhancement. In particular, totally symmetric vibrations, which coincide with the change in molecular geometry under electronic excitations (the Albrecht A term of RRS intensity[49]), are strongly enhanced. According to the TD-DFT calculation of an electronic transition of an R6G molecule that is excited at 488 nm of incident light for Raman excitation, the calculated ($S_0 \rightarrow S_1$) excitation energy (2.913 eV) corresponds to the main electronic absorption ($\lambda_{max} \approx 520$ nm) of R6G in ethanol solution. This $S_0 \rightarrow S_1$ excitation is assigned to the summation of two different transitions (Figure 5). The major transition corresponds to the promotion of an electron from the highest occupied orbital (ϕ_{118}) to the lowest unoccupied xanthene π orbital (ϕ_{119}), and the minor corresponds to a charge transfer (CT) transition from an occupied xanthene

TABLE 2: Calculated and Observed Vibrational Frequencies, and Raman and Infrared Intensities of R6G

	B3LYP/6-311++G(d,p)[a]			experimental ν (cm^{-1})		PED%[b]		B3LYP/6-311++G(d,p)[a]			experimental ν (cm^{-1})		PED%[b]
mode	ν (cm^{-1})	Raman int.	IR int.	Raman	IR	X,A,M,P	mode	ν (cm^{-1})	Raman int.	IR int.	Raman	IR	X,A,M,P
52	610	1.9	43.8		611	X(65),A(20),P(12	104	1191	26.2	43.9		1181	X(88),A(11)
53	615	9.7	12.1	613	615	X(49),P(48)	105	1192	135.7	10.4	1202		X(40),A(10),P(47)
54	631	14.4	3.9	639		X(85),P(14)	106	1239	12.0	177.5		1235	A(13),P(87)
55	664	7.9	5.6	660		X(20),P(80)	107	1259	37.8	380.8		1250	X(39),P(55)
56	673	0.1	2.0	679		X(93)	108	1263	20.6	241.3		1255	X(42),A(11),P(47)
57	697	2.0	1.0			X(86)	109	1265	5.4	27.0			X(71),A(28)
58	702	2.7	0.6	705		X(46),P(52)	110	1271	3.5	4.1			P(95)
59	705	1.6	9.9	705		X(11),P(83)	111	1273	5.2	2.4	1278		P(100)
60	714	1.0	2.1			X(95)	112	1291	149.6	16.2	1294		X(53),A(40)
61	723	1.9	27.0	725	730	X(57),A(33)	113	1301	10.5	38.2			A(17),P(76)
62	737	1.5	17.7	735	740	X(42),P(39)	114	1301	5.9	188.4		1296	X(28),A(72)
63	753	18.5	7.4	741		X(92)	115	1307	119.1	26.9	1312		X(30),A(48),P(21)
64	757	16.6	0.0	746		X(41),A(52)	116	1314	13.9	1197.8		1313	X(59),A(38)
65	771	12.4	0.9	775		X(75),A(11),M(12)	117	1351	351.7	1.4	1364		X(70),A(17)
66	778	1.4	11.1			X(20),A(14),P(60)	118	1360	61.4	93.1		1367	X(17),A(80)
67	794	0.2	0.1			P(98)	119	1365	6.5	11.5			X(43),A(53)
68	803	0.4	14.2			X(16),A(62),P(22)	120	1373	4.7	9.6			P(100)
69	810	0.4	0.1			P(89)	121	1373	20.0	16.4			X(57),A(40)
70	819	6.2	1.7	833		X(35),A(45),P(11)	122	1388	68.0	19.6	1389	1387	A(94)
71	830	0.1	0.2			X(98)	123	1388	23.1	2.6	1389		A(99)
72	830	0.3	42.8		845	X(97)	124	1390	65.0	1.9	1389		M(87)
73	851	11.6	6.2	856		P(95)	125	1392	19.3	2.8	1389		M(95)
74	865	5.1	7.1			P(92)	126	1400	7.0	10.3			P(100)
75	887	11.3	0.3	885		A(86)	127	1419	141.1	119.1	1422	1421	X(69),M(17)
76	891	2.7	4.6			X(10),A(86)	128	1432	17.1	71.0		1446	X(55),A(26),M(17)
77	895	0.4	0.1			X(40),P(51)	129	1445	10.4	7.0			P(96)
78	895	2.7	17.0	903		X(93)	130	1457	9.1	9.0			P(100)
79	897	0.4	0.1			X(54),P(42)	131	1458	37.9	40.4	1450	1452	X(16),A(42),M(42)
80	923	3.8	2.6	936		X(54),A(14),P(32)	132	1458	8.1	16.2			M(97)
81	952	1.3	1.9			X(66),M(20)	133	1459	28.7	21.7			A(15),M(77)
82	978	0.0	0.3			P(97)	134	1462	3.5	1.8			A(95)
83	1004	21.2	1.7	1013		M(79),X(20)	135	1464	5.8	4.9			X(10),A(53),M(37)
84	1007	2.4	46.6		1019	P(100)	136	1466	9.0	29.6			A(94)
85	1011	0.3	2.4			P(98)	137	1467	24.8	0.5	1472		A(97)
86	1014	11.7	94.2	1022	1027	M(58),A(11),P(28)	138	1468	9.8	3.8			P(100)
87	1036	67.8	4.8	1042		X(20),A(68),P(10)	139	1476	2.7	56.3		1477	X(49),A(30),M(21)
88	1042	0.3	1.2			X(21),M(78)	140	1480	46.2	6.5	1490		X(19),M(54),P(20)
89	1042	0.3	0.0			X(21),M(78)	141	1482	44.6	13.0	1490		A(91)
90	1047	20.8	5.2	1061		P(91)	142	1482	4.7	22.8			X(11),A(89)
91	1049	37.7	6.1	1061		X(20),A(78)	143	1486	8.8	11.7			X(10),M(13),P(77)
92	1077	12.1	65.8		1081	A(54),P(36)	144	1488	14.4	3.8			P(94)
93	1084	19.3	130.9	1091		A(37),P(57)	145	1500	7.0	768.8		1501	X(80),M(13)
94	1085	9.0	60.9			A(92)	146	1505	692.0	32.8	1512		X(69),A(25)
95	1110	8.9	8.0	1121	1119	P(98)	147	1530	109.3	369.4	1533	1529	X(87),A(12)
96	1125	47.3	5.7	1130	1129	X(44),A(32),P(14)	148	1554	16.2	77.8			X(72),A(26)
97	1131	3.3	8.0			X(31),A(67)	149	1559	8.2	377.0		1566	X(46),A(54)
98	1137	7.9	17.7	1141		X(21),A(70)	150	1567	89.3	197.1	1559	1557	X(66),A(33)
99	1148	4.1	111.0		1142	P(99)	151	1577	39.0	17.9	1577		P(99)
100	1151	0.3	2.3			P(100)	152	1601	95.0	5.0	1599		P(100)
101	1160	17.8	1.2	1168		X(62),A(22),M(16)	153	1615	103.4	1105.5	1609	1608	X(96)
102	1170	7.9	2.4			P(100)	154	1652	67.7	312.7	1651	1647	X(98)
103	1175	45.4	1.6	1184		X(82),A(14)	155	1716	50.3	292.5	1722	1718	P(100)

[a] Vibrational frequencies scaled by a single factor of 0.9982 are given. Raman intensities are given in units of $Å^4$ amu^{-1}, and infrared intensities in units of km mol^{-1}. [b] Percentage of potential energy distribution (PED%) of normal mode of vibration is given. X refers to the motion of the xanthene ring. A refers to the motion of the NHC_2H_5 groups. M refers to that of a pair of methyl group adjacent to the xanthene ring. P refers to that of the phenyl ring with the $COOC_2H_5$ group. PED% less than 10% is omitted.

π orbital (ϕ_{117}) to an unoccupied phenyl π orbital (ϕ_{121}). Hence, the three RRS signals ν_{55}, ν_{151}, and ν_{154} are strongly enhanced because their vibrational modes would mimic the changes in their molecular geometries between the ground and the resonant excited states. Remarkably, benzene ring vibrational modes (ν_{55} and ν_{151}), which would seem to have no contributions superficially to the main electronic absorption, are largely enhanced in the RRS spectra.

The SERRS spectrum of R6G adsorbed on silver thin film surfaces (Figure 3c) is quite analogous to the RRS spectral pattern of R6G in ethanol solution(Figure 3b). Only a SERRS band at 235 cm^{-1} has no corresponding peak in the RRS spectrum. This band is assigned to the Ag−N stretching mode in accordance with the previous assignments[33] and many other studies of amino compounds adsorbed on silver.[50−52] An enhancement factor estimated from the SERRS/RRS signal ratio at 1650 cm^{-1} (ν_{154}) is approximately 1×10^4 under the same experimental condition, except for the samples with or without silver film. SERRS signals at 1538 cm^{-1} (ν_{147}) and at 1575 cm^{-1} (ν_{151}) relatively increase to the RRS spectral pattern; the factor is, at most, less than 1.5 times normalized by the peak intensity at 1650 cm^{-1} (ν_{154}). No significant changes in Raman frequencies are observed in comparison with the corresponding SERRS and RRS bands. In general, enhancement mechanisms of the surface-enhanced Raman scattering (SERS) are classified into two mechanisms.[53−55] One is an electromagnetic (EM)

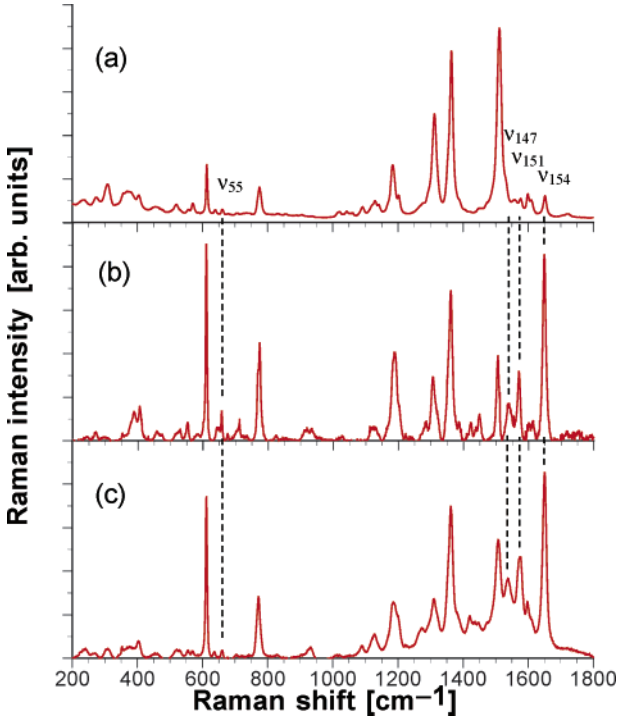

Figure 3. Comparison of the Raman spectra of R6G. (a) The off-resonance Raman spectrum (Ex: 1064 nm) of R6G in ethanol solution, (b) the resonance Raman scattering (RRS) spectrum (Ex: 488 nm) of R6G crystals, and (c) the surface-enhanced resonance Raman scattering (SERRS) spectrum (Ex: 488 nm) of R6G adsorbed on colloidal silver are plotted against the corresponding frequencies (cm^{-1}). The peak assignment of some important peaks (ν_{55}, ν_{147}, ν_{151}, and ν_{154}) is shown.

enhancement mechanism that enhanced whole molecular Raman scatterings due to local surface plasmon polariton.[56−59] Another is a chemical or charge transfer (CT) mechanism that is caused by the changes in the electronic structure of molecules adsorbed on the metal surfaces,[60−62] where the increase of specific SERRS signal and the changes in Raman frequencies against the RRS spectra take place. Therefore, the EM mechanism would be predominant, as for the SERRS measurement of R6G in the present experimental conditions. These results elucidate that adsorption of R6G on the silver surfaces through the Ag−N bonding would be weak and that the molecular orientation of R6G to the silver surfaces might be rather in a random state. This situation is quite similar to that reported by Hildebrandt et al.[33]

D. TERS Spectra of R6G. Figure 6 shows a spectral mapping of the TERS spectra of R6G molecules dispersed on a silver island film using the silver-coated probe tip at 30-nm intervals.[13] Among these TERS spectra, spectra-a, -b, -c, -d, -h, and -i together with spectrum-j (spectra with black lines in Figure 6) are quite similar to the far-field SERRS spectrum (Figure 3c). On the other hand, some of the spectra, such as the spectra-e, -f, and -g (spectra with red lines in Figure 6) exhibit anomalous spectral patterns that are different from those in the far-field SERRS (Figure 3c). Such anomalous spectral patterns, in detail, seem to have an overlap of several new peaks, in addition to the TERS spectral pattern analogous to the far-field SERRS. These anomalies suggest two possible phenomena: one is a case of coexistence of contaminant materials in the anomalous regions of spectra-e, -f, and -g, and another is a case that Raman peaks of R6G molecule itself change in intensities and/or in frequencies. The differential spectrum of spectrum-f (the anomalous region) against spectrum-a (the normal region) was analyzed from the former viewpoint by using a commercial library search (KnowItAll Information System) of Raman peaks. However, no significant results could be obtained from the library search. The anomalous TERS spectrum-f was then compared with the vibrational modes from the latter point of view. The frequencies and relative intensities of the TERS spectrum-f are summarized in Table 3. The frequencies of most TERS bands are consistent with those of the SERRS peaks, although some minor SERRS peaks are missing in the TERS spectrum. In contrast, the intensities of some TERS bands such as bands at 702 cm^{-1} (either ν_{58} or ν_{59}), at 1027 cm^{-1} (ν_{86}), at 1061 cm^{-1} (either ν_{90} or ν_{91}), at 1120 cm^{-1} (ν_{96}), at 1269 cm^{-1} (ν_{111}), and at 1457 cm^{-1} (ν_{131}) are quite inconsistent with those of the SERRS being strongly enhanced.

In the TERS spectra, such as spectra-a, -b, and others drawn in black lines in Figure 6, an averaged enhancement factor by the metallic tip is estimated from the TERS/SERRS signal ratio at 1647 cm^{-1} (ν_{154}).[14] The averaged enhancement factor by the tip reaches approximately 1×10^2 which is extrapolated for the spot area (400 nmϕ) from the metallic tip diameter (40 nmϕ). Meanwhile, a specific enhancement factor is estimated from the signal ratio of the most strongly enhanced peak at 1054 cm^{-1} (ν_{90} or ν_{91}) in spectrum-f. The specific enhancement factor reaches approximately 2×10^4. In TERS spectroscopy, enhancement mechanisms caused by the metallic tip are thought to be the same as the SERS, the EM, and the CT. In addition to these SERS-like enhancement mechanisms, the third mechanism is proposed as a mechanical pressure mechanism due to molecular deformation by the tip;[16] this mechanism does not apply to the case since the mechanical pressure would induce further changes in Raman frequencies against the SERS spectral pattern. According to former two enhancement mechanisms, a ratio of the specific/averaged enhancement factors at least correspond to the contribution of the CT mechanism toward the enhancement. The ratio obtained in the TERS experiment is less than or equal to 10^2; this magnitude is as much as a generally accepted degree of the enhancement effect caused by the CT mechanism.[53−55]

Among the seven peaks of the anomalous TERS signals, two modes (ν_{86} and ν_{131}) are mainly localized in a pair of methyl groups adjacent to the xanthene ring, and four modes (ν_{58}, ν_{59}, ν_{90}, and ν_{111}) are mainly localized in the phenyl region. In short, the vibrating regions of all these vibrational modes are located on the opposite side of the amino group that is bonded to the silver surface. The CT mechanism can be explained by the resonant Raman mechanism in which charge-transfer excitations (either from the metal to the adsorbed molecule, or vice versa) occur at the energy of incident laser frequency.[55] In the case of the TERS, the electronic wave function overlap between the silver atoms of metallic tip apex and molecular orbitals of the adsorbed species is a requirement for the charge-transfer excitations. With an excitation frequency at 488 nm (2.54 eV), adsorbates such as R6G having a narrow HOMO−LUMO band gap are electronically excited from the lower occupied orbitals to a Fermi level of silver surfaces, or from the Fermi level to higher virtual orbitals. In the R6G molecule, occupied orbitals (ϕ_{116} and ϕ_{117}) and a virtual orbital (ϕ_{120}) drawn in Figure 5 are the candidates for the CT electronic excitations in comparison with their energy differences from the Fermi level and the excitation frequency. An electron density distribution of the occupied orbitals (ϕ_{116} and ϕ_{117}) is localized in the xanthene ring, and that of the virtual orbital (ϕ_{120}) is centralized in the phenyl ring. In our Raman NSOM setup, the silver metallic tip approaches from the opposite direction toward the adsorbed R6G molecules on the silver island film and touches the molecules

TABLE 3: Calculated and Experimental Vibrational Frequencies and Raman Intensities of R6G

		experi ment[b]							
	calc[a]	off-res Raman		RRS		SERRS		TERS	
mode	ν (cm^{-1})	ν (cm^{-1})	rel int	ν (cm^{-1})	rel int	ν (cm^{-1})	rel int	ν (cm^{-1})	rel int
53	615	613	0.32	611	1.00	612	0.87	608	0.30
54	631	639	0.00	641	0.00	637	0.03		
55	664	660	0.03	657	0.13	660	0.04		
56	673	679	0.07	675	0.03				
58	702	705	0.09	712	0.11	704	0.02	702	0.15
59	705								
65	771	775	0.16	775	0.58	772	0.33	766	0.30
70	819	833	0.01	826	0.03	830	0.01	808	0.03
78	895	903	0.01	912	0.05	902	0.01		
80	923	936	0.00	934	0.03	931	0.04	919	0.04
86	1014	1022	0.00	1025	0.03	1022	0.01	1027	0.30
90	1047	1061	0.01			1054	0.002	1054	0.35
91	1049								
93	1084	1091	0.03			1090	0.07	1084	0.05
96	1125	1130	0.04	1127	0.06	1127	0.08	1120	0.35
103	1175	1184	0.25	1178	0.51	1185	0.31	1185	0.40
105	1192	1202	0.07	1200	0.07				
111	1273	1278	0.03	1275	0.04	1275	0.05	1269	0.90
112	1291	1294	0.07	1284	0.06				
115	1307	1312	0.47	1310	0.38	1311	0.31	1308	0.30
117	1351	1364	0.80	1361	0.88	1361	0.82	1359	0.70
122	1388	1389	0.07	1385	0.08	1383	0.08		
124	1390								
127	1419	1422	0.04	1422	0.10	1420	0.05		
131	1458	1450	0.04	1450	0.15	1448	0.07	1457	0.65
146	1505	1512	1.00	1505	0.50	1508	0.44	1503	0.30
147	1530	1533	0.11	1536	0.22	1538	0.33	1532	0.45
151	1577	1577	0.07	1577	0.41	1575	0.60	1570	0.70
152	1601	1599	0.09	1600	0.09	1598	0.10	1596	0.03
153	1615	1609	0.08	1612	0.06				
154	1652	1651	0.13	1649	1.00	1650	1.00	1647	1.00
155	1716	1722	0.04	1720	0.03				

[a] Calculated vibrational frequencies of R6G at the B3LYP/6-311++G(*d*,*p*) level. Vibrational frequencies scaled by a factor of 0.9982 are given. [b] Vibrational frequencies of the off-resonance Raman, the resonance Raman (RRS), surface-enhanced resonance Raman (SERRS), and tip-enhanced near-field Raman (TERS) of R6G are given. Spectrum-j, shown in Figure 6, is used for the TERS. Relative intensities for bands of the Raman spectra are normalized with the most intense band in the reported spectral region.

by the contact mode of the AFM standard operation. As the silver atoms of the tip at the apex interact with the virtual orbital (ϕ_{120}) at the phenyl ring of the R6G molecules, the bands (ν_{58}, ν_{59}, and ν_{90}) due to symmetric deforming motions of the phenyl ring could be very highly enhanced in their TERS intensities. Hence, the specific intensity enhancement of some of these TERS bands could be understood with the CT mechanism caused by the silver tip together with the approaching direction of the tip toward the molecule. From the viewpoint of the molecular orientations, it is strongly suggested that R6G molecules in the anomalous regions turn the opposite part of the molecules against the adsorption site to the direction of the metallic tip. In other words, the R6G molecules are in a state of higher order such as assembly or aggregation in the anomalous regions.

The problem concerning enhancement effects on the other anomalous vibrational modes still remains unclear. The TERS band ν_{90} due to a CH_2 twisting motion of the ethyl ester part of the phenyl region is away from the part where the electron density of the virtual orbital ϕ_{120} is significantly high. Accordingly, a large intensity enhancement effect would hardly be expected to the band by means of the CT mechanism. The TERS bands ν_{86} and ν_{131} due to a rocking motion of the methyl group adjacent to the xanthene ring also give the same result. Comparing both the enhancement factors of SERRS/RRS and TERS/SERRS, the averaged enhancement factor of TERS/RRS and the factor at the specific band are estimated to be approximately 1×10^6 and 2×10^8, respectively. In particular, the enhancement factor at the specific band is beyond the values that are usually obtained in the conventional SERS measurement. Recent progress in a single molecule detection of SERS reveals that a gigantic local plasmonic field is generated at a junction between two connecting metallic nanoparticles.[24,28] In our tip-enhanced Raman NSOM, R6G molecules are tightly sandwiched between the silver island film (8-nm thickness) and the silver tip (40 nmϕ) by the contact mode of the AFM. These contacting areas could be the junctions (hot spots). Supposing that the hot spot is an area where all particles (40 nmϕ) are contacting within the gap of 1 nm, the diameter of the hot spot area would be less than 1 nm on the basis of the finite difference time domain (FDTD) method.[18,28] Accordingly, the enhancement factor at the specific band would reach the $10^{11}-10^{12}$ level which is estimated for the conventional TERS observable area by the area of the hot spot. This means a metallic tip-surface doubly enhanced Raman scattering has a possibility to detect the molecular vibration of sub-nanometer size at the level of single molecule. Under such a strong electric field, two enhancement mechanisms would be tentatively considered. One is an extended CT mechanism where the bands of SERRS inactive vibrational modes could be enhanced either with a vibronic coupling (the Albrecht B term[49]) or with electronic excitations that are not excited by the classical, linear CT

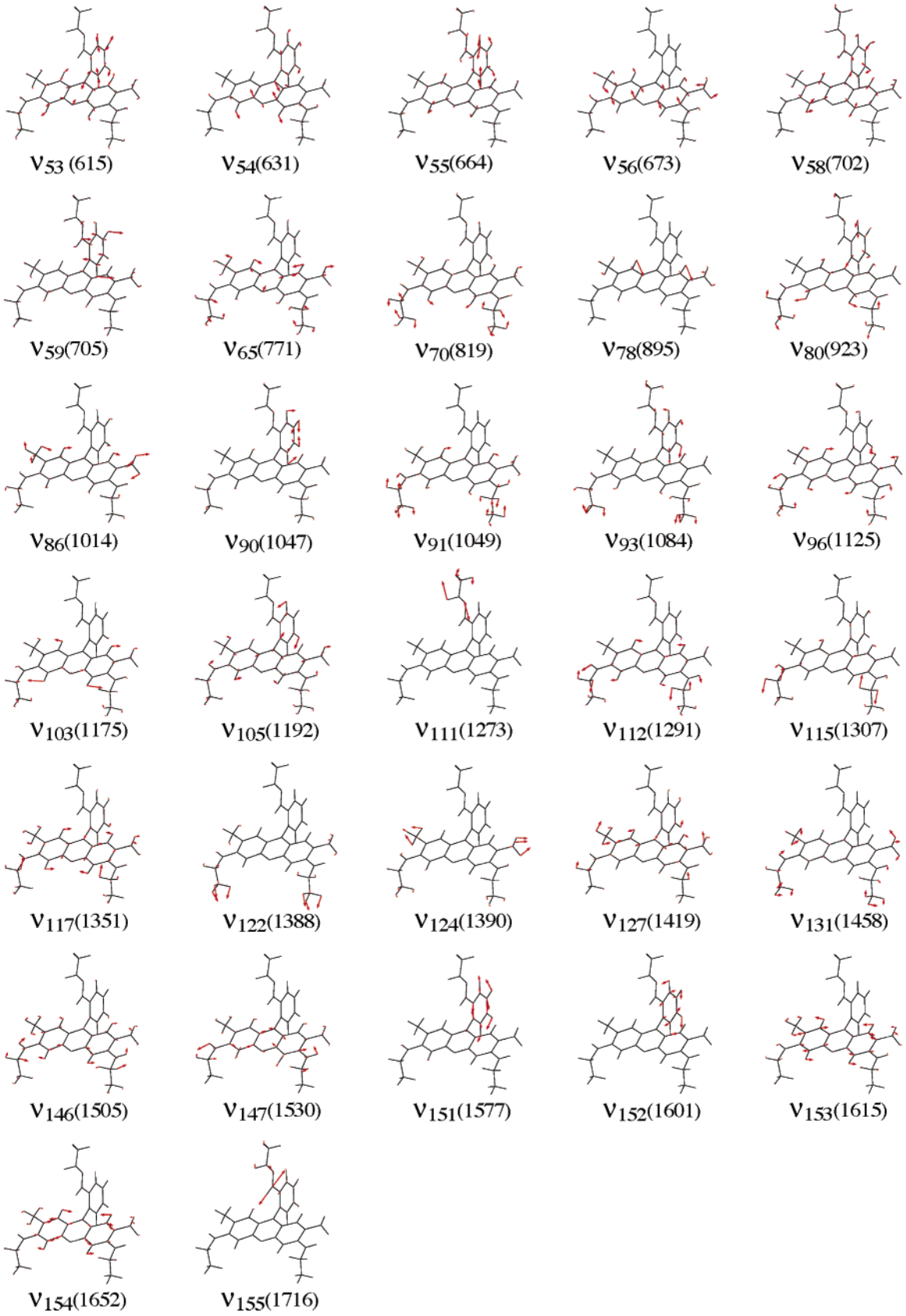

Figure 4. Vibrational patterns of the normal modes of R6G. Mode numbers and calculated frequencies scaled by a single factor of 0.9982 [B3LYP/6-311++G(*d*,*p*)] are given to each mode. Frequencies are given in cm^{-1}.

mechanism. Another is a polarized EM mechanism where Raman bands could be enhanced by a highly polarized electric field coupled with their Raman polarizability tensors. Intensity fluctuation of specific vibrational modes of R6G was reported in the single molecule Raman detection,[16,17] and the calculated polarizability tensors of the specific Raman bands of the R6G

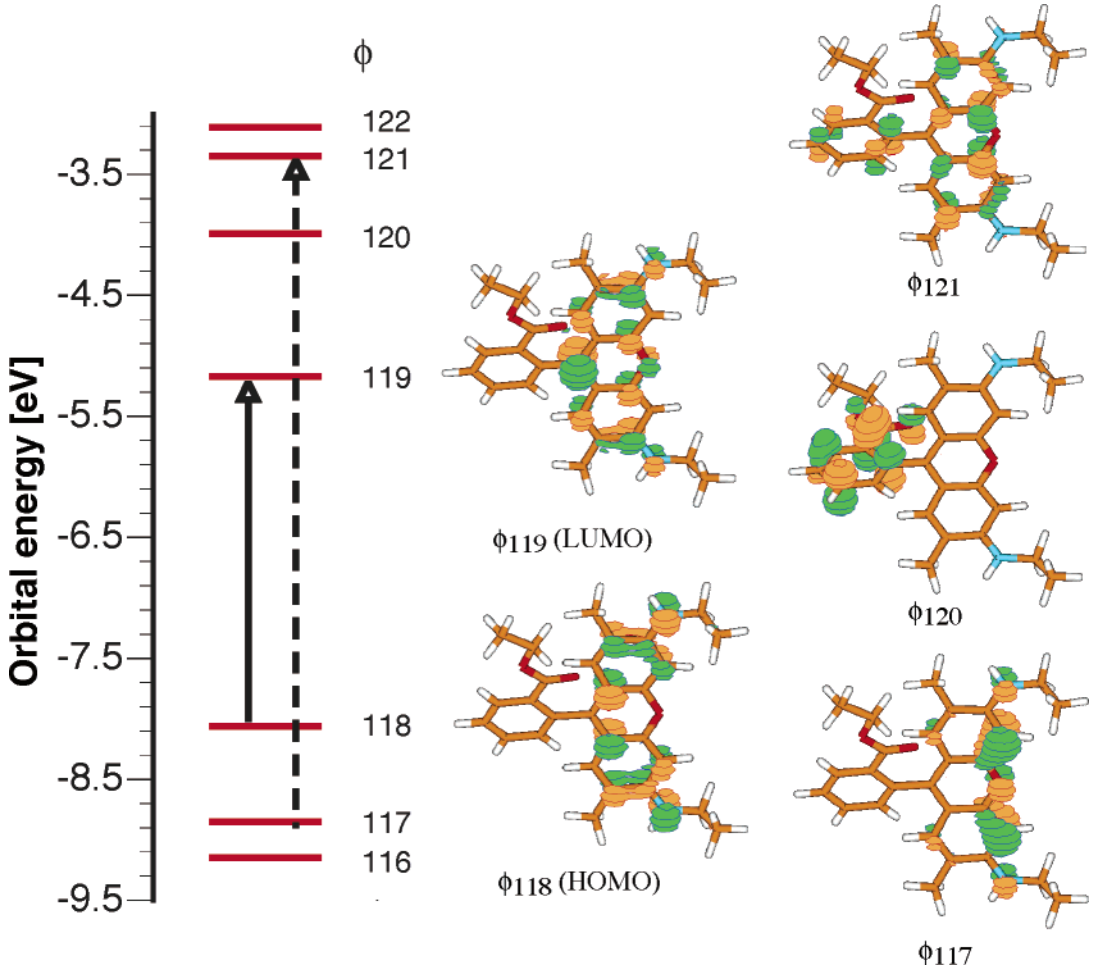

Figure 5. Energy level diagram of $S_0 \rightarrow S_1$ electronic excitation (oscillator strength of 0.7445) of the R6G molecule calculated at the TD-B3LYP/6-311++G(*d*,*p*) level. The corresponding frontier Kohn−Sham orbitals (ϕ_{117}, ϕ_{118}, ϕ_{119}, ϕ_{121}, and ϕ_{121}) of the R6G ground state are depicted.

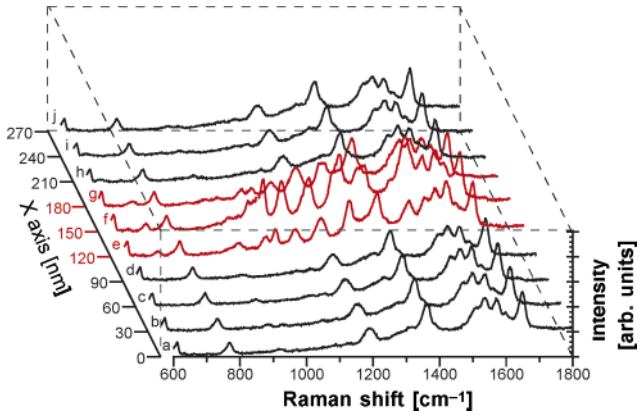

Figure 6. TERS spectral mapping of R6G adsorbed on silver film at several positions. Alphabets (a−j) correspond to the tip position where the TERS spectra were observed.

molecule are parallel to the approaching direction of the tip. However, these evidences are just circumstantial and we have to investigate the actual nature of the enhancement mechanism.

4. Concluding Remarks

The Raman and infrared bands of the R6G molecule are satisfactorily assigned in the region of 1800−600 cm^{-1} on the basis of DFT calculations employing a high-level basis set. By performing TD-DFT calculations of the electronic excited states of R6G in addition to these assignments of the vibrational modes, spectral changes in RRS and SERRS against the normal Raman signals of R6G are investigated. The spectral changes in RRS are briefly discussed in relation to the enhanced vibrational modes and the corresponding electronic excitations. Furthermore, specific enhancement factors observed in the TERS spectra are carefully estimated. These enhancement mechanisms are presumed to be a result of mainly the conventional CT mechanism of SERS in combination with the approaching direction of the metallic probe tip of the Raman NSOM toward adsorbed R6G molecules. In addition, we propose novel further enhancement mechanisms capable of sensing molecular vibrations of sub-nanometer size at the single molecule level. Although detailed enhancement mechanisms are unclear, a technique of the tip-surface doubly enhanced near-field Raman spectroscopy would be able to detect molecular distributions and orientations at sub-nanometer size beyond the spatial resolution achieved by the conventional near-field spectroscopy.

Acknowledgment. The authors gratefully thank Dr. Prabhat Verma for his valuable comments on this work. One of the authors (Y.I.) also gratefully acknowledges financial support by a Grant-in-Aid for Scientific Research No. 16360034 from the Ministry of Education, Culture, Sports, Science and Technology.

References and Notes

(1) Tsai, D. P.; Othonos, A.; Moskovits, M.; Uttamchandani, D. *Appl. Phys. Lett*. **1994**, *64*, 1768.

(2) Jahncke, C. L.; Paesler, M. A.; Hallen, H. D. *Appl. Phys. Lett*. **1995**, *67*, 2483.

(3) Smith, D. A.; Webster, S.; Ayad, M.; Evans, S. D.; Fogherty, D.; Batchelder, D. *Ultramicroscopy* **1995**, *61*, 247.
(4) Inouye, Y.; Hayazawa, N.; Hayashi, K.; Sekkat, Z.; Kawata, S. In *Proc. of SPIE, Denver*; **1999**, *3791*, 40.
(5) Hayazawa, N.; Inouye, Y.; Sekkat, Z.; Kawata, S. *Opt. Commun*. **2000**, *183*, 333.
(6) Stöckle, R. M.; Suh, Y. D.; Deckert, V.; Zenobi, R. *Chem. Phys. Lett*. **2000**, *318*, 131.
(7) Anderson, M. S. *Appl. Phys. Lett*. **2000**, *76*, 3130.
(8) Pohl, D. W.; Denk, W.; Lanz, M. *Appl. Phys. Lett*. **1984**, *44*, 651.
(9) Harootunian, A.; Betzig, E.; Isaacson, M.; Lewis, A. *Appl. Phys. Lett*. **1986**, *49*, 674.
(10) Betzig, E.; Chichester, R. J. *Science* **1993**, *262*, 1422.
(11) Xie, X. S.; Dunn, R. C. *Science* **1994**, *265*, 361.
(12) Ambrose, W. P.; Goodwin, P. M.; Martin, J. C.; Keller, R. A. *Science* **1994**, *265*, 364.
(13) Hayazawa, N.; Inouye, Y.; Sekkat, Z.; Kawata, S. *Chem. Phys. Lett.* **2001**, *335*, 369.
(14) Hayazawa, N.; Inouye, Y.; Sekkat, Z.; Kawata, S. *J. Chem. Phys*. **2002**, *117*, 1296.
(15) Hayazawa, N.; Yano, T.; Watanabe, H.; Inouye, Y.; Kawata, S. *Chem. Phys. Lett*. **2003**, *376*, 174.
(16) Watanabe, H.; Ishida, Y.; Hayazawa, N.; Inouye, Y.; Kawata, S. *Phys. Rev. B* **2004**, *69*, 155418.
(17) Fischer, U. Ch.; Pohl, D. W. *Phys. Rev. Lett*. **1989**, *62*, 458.
(18) Inouye, Y.; Kawata, S. *Opt. Lett*. **1994**, *19*, 159.
(19) Novotny, L.; Sanchez, E. J.; Xie, X. S. *Ultramicrscopy* **1998**, *71*, 21.
(20) Furukawa, H.; Kawata, S. *Opt. Commun.* **1998**, *148*, 221.
(21) Chang, R. F.; Furtak, T. E. *Surface Enhancement Raman Scattering*; Plenum: New York, 1982.
(22) Nie, S.; Emory, S. R. *Science* **1997**, *275*, 1102.
(23) Kneipp, K.; Wang, Y.; Kneipp, H.; Perelman, L. T.; Itzkan, I.; Dasari, R. R.; Feld, M. S. *Phys. Rev. Lett.* **1997**, *78*, 1667.
(24) Michaels, A. M.; Nirman, M.; Brus, L. E. *J. Am. Chem. Soc.* **1999**, *121*, 9932.
(25) Gunnarsson, L.; Bjerneld, E. J.; Xu, H.; Petronis, S.; Kasemo, B.; Käll, M. *Appl. Phys. Lett*. **2001**, *78*, 802.
(26) Meixner, A. J.; Vosgröne, T.; Sackrow, M. *J. Lumin.* **2001**, *94*−*95*, 147.
(27) Weiss, A.; Haran, G. *J. Phys. Chem. B* **2001**, *105*, 12348.
(28) Futamata, M.; Maruyama, Y.; Ishikawa, M. *J. Phys. Chem. B* **2003**, *107*, 7607.
(29) Li, W.-H.; Li, X.-Y.; Yu, N.-T. *Chem. Phys. Lett.* **1999**, *312*, 28.
(30) Hayashi, M.; Lin, S. H.; Baschke, M. B.; Shen, Y. R. *J. Phys. Chem. A* **2002**, *106*, 2271.
(31) Emory, S. R.; Nie, S. *Anal. Chem*. **1997**, *69*, 2631.
(32) Zeisel, D.; Deckert, V.; Zenobi, R.; Vo-Dinh, T. *Chem. Phys. Lett*. **1998**, *283*, 381.
(33) Hildebrandt, P.; Stockburger, M. *J. Phys. Chem*. **1984**, *88*, 5935.
(34) Becke, A. D. *J. Chem. Phys*. **1993**, *98*, 5648.
(35) Lee, C.; Yang, W.; Parr, R. *G. Phys. Rev. B* **1988**, *37*, 785.
(36) Bauernschmitt, R.; Ahlrichs, R. *Chem. Phys. Lett*. **1996**, *256*, 454.
(37) Casida, M. E.; Jamorski, C.; Casida, K. C.; Salahub, D. R. *J. Chem. Phys*. **1998**, *108*, 4439.
(38) Frisch, M. J.; Trucks, G. W.; Schlegel, H. B.; Scuseria, G. E.; Robb, M. A.; Cheeseman, J. R.; Zakrzewski, V. G.; Montgomery, J. A., Jr.; Stratmann, R. E.; Burant, J. C.; Dapprich, S.; Millam, J. M.; Daniels, A. D.; Kudin, K. N.; Strain, M. C.; Farkas, O.; Tomasi, J.; Barone, V.; Cossi, M.; Cammi, R.; Mennucci, B.; Pomelli, C.; Adamo, C.; Clifford, S.; Ochterski, J.; Petersson, G. A.; Ayala, P. Y.; Cui, Q.; Morokuma, K.; Malick, D. K.; Rabuck, A. D.; Raghavachari, K.; Foresman, J. B.; Cioslowski, J.; Ortiz, J. V.; Baboul, A. G.; Stefanov, B. B.; Liu, G.; Liashenko, A.; Piskorz, P.; Komaromi, I.; Gomperts, R.; Martin, R. L.; Fox, D. J.; Keith, T.; Al-Laham, M. A.; Peng, C. Y.; Nanayakkara, A.; Challacombe, M.; Gill, P. M. W.; Johnson, B.; Chen, W.; Wong, M. W.; Andres, J. L.; Gonzalez, C.; Head-Gordon, M.; Replogle, E. S.; Pople, J. A. *Gaussian 98*, revision A.9; Gaussian, Inc.: Pittsburgh, PA, 1998.
(39) Mohandas, P.; Umapathy, S. *J. Phys. Chem. A* **1997**, *101*, 4449.
(40) Schaftenaar, G.; Noordik, J. H. *J. Comput.-Aided Mol. Des*. **2000**, *14*, 123.
(41) Yamakita, Y. *LXVIEW*; The University of Tokyo: Tokyo, Japan, 1995.
(42) Okamoto, Y. *VLX*; Fuji Photo Film. Co., Ltd.: Kanagawa, Japan, 2001.
(43) Adhikesavalu, D. N.; Mastropaolo, D.; Camerman, A.; Camerman, N. *Acta Cryst*. **2001**, *C57*, 657.
(44) Rauhut, G.; Pulay, P. *J. Phys. Chem.* **1995**, *99*, 3093.
(45) Yoshida, H.; Ehara, A.; Matsuura, H. *Chem. Phys. Lett*. **2000**, *325*, 477.
(46) Watanabe, H.; Okamoto, Y.; Furuya, K.; Sakamoto, A.; Tasumi, M. *J. Phys. Chem. A* **2002**, *106*, 3318.
(47) Yoshida, H.; Takeda, K.; Okamura, J.; Ehara, A.; Matsuura, H. *J. Phys. Chem. A* **2002**, *106*, 3580.
(48) Clarkson, J.; Smith, W. E.; Batchelder, D. N.; Smith, D. A.; Coats, A. M. *J. Mol. Struct*. **2003**, *648*, 203.
(49) Albrecht, A. C. *J. Chem. Phys.* **1961**, *34*, 1476.
(50) Lombardi, J. R.; Shields Knight, E. A.; Birke, R. L. *Chem. Phys. Lett*. **1981**, *79*, 214.
(51) Neto, N.; Muniz-Miranda, M.; Sbrana, G. *J. Phys. Chem*. **1996**, *100*, 9911.
(52) Otto, C.; van den Tweel, T. J. J.; de Mul, F. F. M.; Greve, J. *J. Raman Spectrosc*. **1986**, *17*, 289.
(53) Moskovits, M. *Rev. Mod. Phys*. **1985**, *57*, 783.
(54) Otto, A.; Mrozek, I.; Grabhorn, H.; Akemann, W. J. *J. Phys.: Condens. Matter* **1992**, *4*, 1143.
(55) Campion, A.; Kambhampati, P. *Chem. Soc. Rev*. **1998**, *27*, 241.
(56) King, F. W.; Van Duyne, R. P.; Schatz, G. C. *J. Chem. Phys*. **1978**, *69*, 4472.
(57) Efrima, S.; Metiu, H. *J. Chem. Phys.* **1979**, *70*, 1939.
(58) Creighton, J. A. *Surf. Sci*. **1983**, *124*, 209.
(59) Otto, A.; Timper, J.; Billmann, J.; Kovacs, G.; Pockrand, I. *Surf. Sci*. **1980**, *92*, L55.
(60) Billmann, J.; Kovacs, G.; Otto, A. *Surf. Sci*. **1980**, *92*, 153.
(61) Otto, A.; Billmann, J.; Eickmans, J.; Ertuerk, U.; Pettenkofer, C. *Surf. Sci*. **1984**, *138*, 319.
(62) Campion, A.; Ivanecky, J. E., III; Child, C. M.; Foster, M. *J. Am. Chem. Soc*. **1995**, *117*, 11807.